

Intriguing Properties of Positional Encoding in Time Series Forecasting

Jianqi Zhang, Jingyao Wang, Wenwen Qiang, Fanjiang Xu, Changwen Zheng, Fuchun Sun, *Fellow, IEEE*, and Hui Xiong, *Fellow, IEEE*

Abstract—Transformer-based methods have made significant progress in time series forecasting (TSF). They primarily handle two types of tokens, i.e., temporal tokens that contain all variables of the same timestamp, and variable tokens that contain all input time points for a specific variable. Transformer-based methods rely on positional encoding (PE) to mark tokens' positions, facilitating the model to perceive the correlation between tokens. However, in TSF, research on PE remains insufficient. To address this gap, we conduct experiments and uncover intriguing properties of existing PEs in TSF: (i) The positional information injected by PEs diminishes as the network depth increases; (ii) Enhancing positional information in deep networks is advantageous for improving the model's performance; (iii) PE based on the similarity between tokens can improve the model's performance. Motivated by these findings, we introduce two new PEs: Temporal Position Encoding (T-PE) for temporal tokens and Variable Positional Encoding (V-PE) for variable tokens. Both T-PE and V-PE incorporate geometric PE based on tokens' positions and semantic PE based on the similarity between tokens but using different calculations. To leverage both the PEs, we design a Transformer-based dual-branch framework named T2B-PE. It first calculates temporal tokens' correlation and variable tokens' correlation respectively and then fuses the dual-branch features through the gated unit. Extensive experiments demonstrate the superior robustness and effectiveness of T2B-PE. The code is available at: <https://github.com/jlu-phylComputer/T2B-PE>.

Index Terms—Time series forecasting, Transformer-based methods, positional encoding

I. INTRODUCTION

TIME series forecasting (TSF) is essential in numerous practical applications, e.g., weather forecasting [1]–[3], energy planning [4]–[6], financial prediction [7]–[9] and traffic flow forecasting [10]–[12]. Recent advancements have been made with Transformer-based methods [13]–[15], which mainly take as input two types of tokens: (i) temporal tokens, which contain all variables of the same timestamp; (ii) variable tokens, which contain all input time points for a specific variable. Temporal tokens derive their significance from temporal variations, e.g., the trend, periodicity, and peak valley [16],

J. Zhang, J. Wang, W. Qiang, F. Xu, and C. Zheng are with the University of Chinese Academy of Sciences, Beijing, China. They are also with the National Key Laboratory of Space Integrated Information System, Institute of Software Chinese Academy of Sciences, Beijing, China. E-mail: jlu-zhangjianqi@163.com, wangjingyao2023@iscas.ac.cn, qiangwenwen@iscas.ac.cn, fanjiang@iscas.ac.cn, changwen@iscas.ac.cn.

F. Sun is with the Science & Technology on Integrated Information System Laboratory, Department of Computer Science and Technology, Tsinghua University, Beijing, China. E-mail: fcsun@tsinghua.edu.cn.

H. Xiong is with the Hong Kong University of Science and Technology, China. E-mail: xionghui@ust.hk.

Jianqi Zhang and Jingyao Wang have contributed equally.

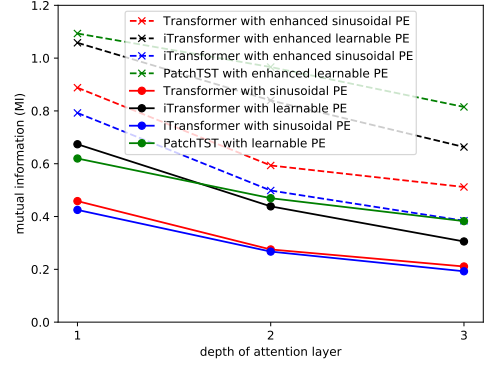


Fig. 1. Illustration of the change in the Mutual Information (MI) between the PE and the input embedding of each attention layer with the depth of the attention layer. The solid line represents the results of the method with normal PE, while the dashed line represents the results of the method with our enhanced PE.

while variable tokens' significance comes from multivariate correlation [15].

The attention mechanism in Transformers is permutation-invariant, which discards the position information of the tokens in an input sequence [17]. Without the position information of tokens, the model can't perceive temporal variations or identify variable tokens well, hindering its ability to compute temporal and multivariate correlation [18], [19]. Previous works [19]–[23] have introduced positional encoding (PE) e.g., sinusoidal PE [24] and learnable PE [25], to mitigate this issue. Generally, in transformer-based TSF methods, PE is only applied at the input layer [20]–[23]. However, with the deepening of neural network layers, the information of initial input gradually diminishes [26]. This brings **the first question** regarding PE: Does the amount of positional information decrease with an increase in the number of network layers? If the first question holds true, **the second question** about PE is: Is enhancing positional information in deep networks advantageous for improving model performance? Meanwhile, absolute positional information can be considered as the proximity relationship of different tokens in geometric space. Without causing confusion, we refer to this type of PE which encodes tokens' positions as geometric PE. The proximity relationship can also be obtained based on the semantic similarity between different tokens. Therefore, based on this similarity, we propose a new type of PE, called semantic PE. The geometric PE, which is related to the subjectively divided positions of tokens, is therefore

unstable. In contrast, the semantic PE considers the content of the token, unaffected by human intervention, and possesses invariance. Therefore, **the third question** about PE is: In the semantic space, can the semantic PE enhance the model's performance like the geometric PE?

To explore these three questions, we construct three sets of experiments. **For the first question**, we evaluate the Mutual Information (MI) [27] between the PE and the input embedding of each attention layer to observe the change of positional information. MI is an information-theoretic measure that quantifies the degree of dependency between two variables [26]. It can quantify the amount of information one variable contains about another. A higher MI means the two variables are more closely linked. Therefore, the MI between the PE and the input embedding of each attention layer can reveal how much positional information the latter contains. The calculation method for the MI between two continuous variables is detailed in the Appendix. We train multiple models on the Weather dataset and the ECL dataset in [15] to record the above MI. As shown in Figure 1, we find that as the layer of the network deepens, the MI decreases. Therefore, the amount of positional information decreases with an increase in the number of network layers. **For the second question**, we evaluate multiple models after adding PE to the input embedding of each attention layer which we called the enhanced PE, exploring the impact of enhancing positional information. We find that the enhanced PE not only alleviates the phenomenon mentioned above (Figure 1) but also improves models' performance (Table I). Therefore, enhancing positional information in deep networks is advantageous for improving model performance. **For the third question**, we evaluate multiple models after adding the semantic PE to explore its effects. We find that this strategy improves prediction performance (Table I), which indicates the effectiveness of the semantic PE.

Based on the above observations, we propose two new types of PEs: temporal positional encoding (T-PE) for temporal tokens and variable positional encoding (V-PE) for variable tokens. T-PE consists of geometric PE and semantic PE. The geometric PE is the enhanced PE used in the above experiments, whose rationality has been confirmed. The semantic PE is calculated based on the similarity of initial tokens to maintain the semantic similarity between different tokens in the input space. These initial tokens are the ones that have not undergone any attention layer processing. V-PE consists of another type of geometric PE and semantic PE. Specifically, the geometric PE in V-PE is generated through convolution, while the semantic PE is the same as that of T-PE. To leverage both T-PE and V-PE, we develop a novel Transformer-based dual-branch framework called T2B-PE. T2B-PE first separately handles the correlations between temporal tokens and the correlations between variable tokens and then combines the dual-branch features using a novel gated unit designed for TSF to predict the results. Each branch utilizes the encoder of the vanilla Transformer with the newly proposed PEs. Extensive experiments demonstrate the superior robustness and effectiveness of T2B-PE. Our contributions are as follows:

- We discover three conclusions for Transformer-based TSF methods, i) the amount of positional information decreases

with an increase in the number of network layers; ii) enhancing positional information in deep networks is advantageous for improving model performance; iii) both geometric PE and semantic PE can contribute to enhancing model performance.

- We design two novel PEs for more efficient TSF: T-PE for temporal tokens and V-PE for variable tokens. To leverage both the T-PE and V-PE, we develop a simple but powerful Transformer-based dual-branch framework (T2B-PE) to process temporal and variable tokens separately and fuse the processed results.
- Extensive experiments conducted on six benchmark datasets demonstrate the superior robustness and effectiveness of our proposed T2B-PE and two PEs.

II. RELATED WORK

Transformer-based TSF methods using temporal tokens:

Most TSF methods belong to this category, e.g., Informer [21], Autoformer [28], FedFormer [29], PeriodFormer [30], GCformer [31], Preformer [32], MANF [33], PromptCast [34] and Infomaxformer [35]. The core of these methods is to use the correlation between temporal tokens to predict future data.

Transformer-based TSF methods using variable tokens:

This type of method mainly has recently emerged which only contains iTransformer [15]. Although iTransformer solely utilizes the correlation between variable tokens to predict future data, its authors also explicitly state that the correlation between temporal tokens and the correlation between variable tokens is equally important. Additionally, iTransformer does not incorporate any PE for variable tokens. This is unreasonable. From our experiments (Table I), it can be seen that simply adding PE to the variable tokens of iTransformer can significantly improve its predictive performance.

Transformer-based TSF methods using both temporal tokens and variable tokens: This type of method has recently become very popular, such as Crossformer [19], DSformer [36]. These methods utilize both the correlation between variable tokens and the correlation between temporal tokens to predict future data. Among them, Crossformer assigns PE to both temporal tokens and variable tokens, while DSformer does not mention any details related to PE.

PE in Transformer-based TSF methods: In TSF, there hasn't been sufficient attention from the academic community on PE. Nearly all algorithms employ either the learnable PE similar to Bert [25] or the sinusoidal PE similar to Transformer [24]. In this paper, we aim to explore the previously overlooked intriguing properties of PEs mentioned in Section I, and then design the most suitable and efficient PEs for temporal tokens and variable tokens.

III. MOTIVATION

In this section, we provide detailed experimental results and analysis for the three experiments mentioned in Section I.

In the first experiment, we use the Weather dataset and the ECL dataset in [15] to train three methods: vanilla Transformer [24], PatchTST [20] and iTransformer [15] with the sinusoidal PE or the learnable PE. Vanilla Transformer and PatchTST

TABLE I
EXPERIMENTAL RESULTS ON THE WEATHER DATASET AND THE ECL DATASET WITH DIFFERENT PEs. FOR MORE DETAILS, PLEASE REFER TO APPENDIX C.

MSE/MAE	Dataset	Original	+enhanced PE	+semantic PE
Transformer+sinusoidal PE	Weather	0.379/0.432	0.339/0.393	0.347/0.400
	ECL	0.333/0.414	0.289/0.381	0.313/0.391
PatchTST+learnable PE	Weather	0.259/0.281	0.250/0.274	0.255/0.276
	ECL	0.216/0.304	0.211/0.298	0.213/0.300
iTransformer+sinusoidal PE	Weather	0.255/0.278	0.254/0.277	0.248/0.276
	ECL	0.174/0.267	0.171/0.266	0.168/0.263
iTransformer+learnable PE	Weather	0.251/0.276	0.249/0.276	0.245/0.274
	ECL	0.176/0.268	0.173/0.267	0.170/0.265
iTransformer(w/o PE)	Weather	0.258/0.279	-	-
	ECL	0.178/0.270	-	-

only deal with temporal tokens, and iTransformer solely deals with variable tokens. In this experiment, the lookback length is 96 and the prediction lengths $\in \{96, 192, 336, 720\}$. The number of encoder layers is set to 3 for all algorithms. We compute the MI between the PE and the input embedding of each attention layer. For each layer of every algorithm, the MI of all samples is averaged. The results presented in Figure 1 suggest that as the depth of the network increases, there is a decrease in the amount of positional information, as indicated by the decreasing MI.

In the second experiment, we explore whether enhancing the positional information in deep networks benefits model performance. Specifically, we use the Weather dataset and the ECL dataset in [15] as the benchmark datasets and select the same three models in the first experiment as baselines. The lookback length is set to 96 and the prediction lengths are set to $\{96, 192, 336, 720\}$. Next, after adding enhanced PE, we train the models under different prediction lengths in turn and record the average mean squared error (MSE), the average mean absolute error (MAE), and the MI. The results are illustrated in Table I and Figure 1. From the results, we observe that enhanced PE mitigates the phenomenon of positional information decay mentioned in the first experiment and improves the models' performance. This suggests that enhancing the positional information in deep networks is beneficial for improving model performance.

In the third experiment, we explore whether the semantic PE can also improve the model's performance. The geometric PE is solely related to the token's position, enabling the identification of its neighbors for any given token based on position. However, token positions are manually assigned and susceptible to external factors and the data collection process, which makes them unstable. Conversely, without considering the order, neighbors for each token can be identified based on the semantic similarity of tokens, that is, similar tokens are close, and dissimilar tokens are far apart. Therefore, differing from geometric PE, we propose using a matrix based on the similarity between initial tokens to represent semantic PE. Considering the structure of the transformer, we apply semantic PE in the attention mechanism. Specifically, we apply the same experimental settings as the second experiment but insert semantic PE instead of enhanced PE. Then, we record the

MSE and MAE results, as shown in Table I. From the result, we observe that semantic PE decreases both the MSE and MAE. It illustrates that semantic PE can also enhance model performance as geometric PE does.

Through the above conclusions, we can further obtain that (i) in TSF, the information provided by commonly used PEs in the current Transformer-based methods is insufficient; (ii) both the geometric PE and the semantic PE can better enhance the performance of the Transformer-based TSF models. These conclusions inspire us to design more effective PEs on temporal tokens and variable tokens.

IV. METHOD

In this section, we first introduce the notation in Section IV-A. Next, we present the "Temporal Tokens with T-PE" and "Variable Tokens with V-PE" in Section IV-B and Section IV-C, respectively. Finally, we introduce the proposed Transformer-based dual-branch framework (T2B-PE) in Section IV-D.

A. Notation

In TSF, given historical observations $X = \{\mathbf{x}_1, \dots, \mathbf{x}_T\} \in \mathbb{R}^{T \times N}$ with T timestamps and N variables, we predict the future S timestamps $Y = \{\mathbf{x}_{T+1}, \dots, \mathbf{x}_{T+S}\} \in \mathbb{R}^{S \times N}$. Here, T denotes the lookback length, while S denotes the prediction length. For convenience, we denote $X_{t,:}$ as the simultaneously recorded multivariate at timestamp t , and $X_{:,n}$ as the whole time series of each variable indexed by n .

B. Temporal Tokens with T-PE

In this subsection, we introduce the temporal tokens with the proposed temporal positional encoding (T-PE). T-PE consists of geometric PE and semantic PE. Specifically, the geometric PE focuses on the positional information between tokens. It enhances positional information in deep networks through the proposed enhanced PE. The semantic PE centers on the similarity between initial tokens. It aims to inject semantic proximity relationships.

For the geometric PE of T-PE, an intuitive idea is to use the enhanced PE strategy mentioned in Section I. In general, there are two types of geometric PE in time series, e.g., sinusoidal PE and learnable PE. According to [25], when the dataset is sufficiently large, learnable PE performs better; conversely, sinusoidal PE is more effective. In this study, since the used TSF datasets are not large, we use enhanced sinusoidal PE as the geometric PE of T-PE. The semantic PE in T-PE is designed based on the similarity of initial tokens, which aims to preserve the semantic similarity between different tokens. The semantic PE can be regarded as a similarity matrix of initial tokens, while geometric PE is generated based on positional indices. This fundamental difference leads to the fact that the semantic PE cannot be directly added to input embeddings in the same way as the geometric PE. Since attention maps also represent the similarity between tokens and have a shape consistent with the similarity matrix between initial tokens, we inject semantic PE into the attention maps. Specifically, we use an L2 regularization term to constrain the difference

between the attention maps at each layer and the similarity matrix between initial tokens.

Next, we introduce the generation of temporal tokens with T-PE. To begin with, we generate initial temporal tokens, each of which is obtained as follows:

$$h_t^{time} = \text{Embed}^t(X_{t,:}) + PE_t, \quad t = 1, 2, \dots, T, \quad (1)$$

$$s.t. \quad PE_{t,2i} = \sin\left(\frac{t}{10000 \frac{2i}{D}}\right), PE_{t,2i+1} = \cos\left(\frac{t}{10000 \frac{2i}{D}}\right),$$

where t is the position, $h_t^{time} \in \mathbb{R}^D$, D is the dimension of tokens, $\text{Embed}^t(\mathbb{R}^N \rightarrow \mathbb{R}^D)$ is implemented by a multi-layer perceptron, $PE_t \in \mathbb{R}^D$ is the sinusoidal PE in [24], and $i \in \{0, 1, 2, \dots, D/2 - 1\}$ represents the index of the dimension. We refer to $H^{time} = \{h_1^{time}, \dots, h_T^{time}\}$ as the initial temporal tokens. After obtaining the temporal tokens, we add the sinusoidal PE to the input embedding of each attention layer to insert the enhanced sinusoidal PE. Assuming the input embedding of the l -th attention layer is H_l^{time} , where H_1^{time} is H^{time} , the input embedding with the enhanced sinusoidal PE becomes:

$$H_l^{en-time} = H_l^{time} + PE_t. \quad (2)$$

Note that enhancing positional information in V dilutes token features which reduces the model's performance. Enhancing positional information in Q and K doesn't dilute token features since they are only for calculating tokens' attention maps. Thus, the generation of Q and K in the attention mechanism depends on the $H_l^{en-time}$, while the generation of V depends on the H_l^{time} . We validate the effectiveness of this mechanism through experiments in Section V-C. From this process, we insert the geometric PE of T-PE into temporal tokens.

To insert the semantic PE of T-PE into temporal tokens, we propose an L2 regularization term \mathcal{L}_{sem}^{time} to constrain the difference between the attention maps at each layer and the similarity matrix between initial tokens, expressed as:

$$\mathcal{L}_{sem}^{time} = \sum_{l=1}^L \ell_2\left[\delta\left(\frac{Q_l^{time} K_l^{time\top}}{\sqrt{D}}\right), \delta\left(\frac{H^{time} H^{time\top}}{\sqrt{D}}\right)\right], \quad (3)$$

where L is the number of attention layers in the model, $\ell_2[\dots]$ is the L2 distance, δ is the softmax operation, δ is the operation of the softmax, $\delta(Q_l^{time} K_l^{time\top} / \sqrt{D})$ denotes the attention map in l -th attention layer and $\delta(H^{time} H^{time\top} / \sqrt{D})$ is the similarity matrix of initial temporal tokens. The injection way of the semantic PE significantly diverges from that of traditional geometric PEs. However, both serve a similar purpose: they embed proximity relations among tokens into the model. Specifically, the semantic PE infuses these relations within the semantic space, whereas traditional geometric PEs incorporate them within the geometric space.

To this end, we introduce our proposed T-PE and insert it into temporal tokens, which aids the model in better perceiving temporal variations.

C. Variable Tokens with V-PE

In this subsection, we introduce the variable tokens with the proposed variable positional encoding (V-PE). V-PE includes another type of geometric PE and semantic PE. Specifically, the geometric PE focuses on both positional information and token

features, which is the newly proposed time series convolutional PE. The semantic PE is the same as that of T-PE. Next, we provide the details of V-PE.

In TSF, the commonly used PEs, e.g., sinusoidal PE and learnable PE, are based on the absolute position information. These PEs can lead to excessive differentiation between two tokens that are far apart in geometric space but share similar features [17], which is not reasonable for variable tokens. Meanwhile, according to the results shown in Table I, the enhanced PE does not significantly improve iTransformer based on variable tokens. This prompts us to develop a new geometric PE for variable tokens that can consider both absolute position information and the tokens' features. Previous research [17], [37] demonstrates that convolution can consider token features while perceiving positional information. Based on this property, we design time series convolutional PE as the geometric PE of V-PE. For the semantic PE, the variable tokens also use the same semantic PE as Section IV-B in V-PE.

Next, we introduce the generation of variable tokens with V-PE. To begin with, we generate initial variable tokens each of which is obtained as follows:

$$h_n^{var} = \text{Embed}^v(X_{:,n}), \quad n = 1, 2, \dots, N, \quad (4)$$

where $h_n^{var} \in \mathbb{R}^D$, $\text{Embed}^v(\mathbb{R}^T \rightarrow \mathbb{R}^D)$ is implemented by a multi-layer perceptron. We refer to $H^{var} = \{h_1^{var}, \dots, h_N^{var}\}$ as the initial variable tokens. Time series convolutional PE employs Depthwise Convolution (DWConv) [38], and is added to the input embedding of each attention layer. Assuming the input embedding of the l -th attention layer is H_l^{var} , where H_1^{var} is H^{var} , the input embedding with time series convolutional PE becomes:

$$H_l^{en-var} = H_l^{var} + \text{DWConv}(H_l^{var}), \quad (5)$$

where, the kernel size of DWConv is set to 3. Time series convolution PE contains the original token's feature, its addition to V doesn't dilute the token's feature. Therefore, the generation of Q , K and V can all depend on H_l^{en-var} . The way to insert semantic PE is also to add a regularization term in the loss function, expressed as:

$$\mathcal{L}_{sem}^{var} = \sum_{l=1}^L \ell_2\left[\delta\left(\frac{Q_l^{var} K_l^{var\top}}{\sqrt{D}}\right), \delta\left(\frac{H^{var} H^{var\top}}{\sqrt{D}}\right)\right], \quad (6)$$

where $\delta(Q_l^{var} K_l^{var\top} / \sqrt{D})$ is the attention map in l -th attention layer. $\delta(H^{var} H^{var\top} / \sqrt{D})$ is the similarity matrix of initial variable tokens.

To this end, we introduce our proposed V-PE and insert it into variable tokens, which aids the model in better perceiving the correlation between variable tokens.

D. T2B-PE

In this subsection, we introduce the Transformer-based dual-branch framework (T2B-PE) which leverages both the T-PE and V-PE mentioned above, thus improving model performance. T2B-PE first handles the correlations between temporal tokens and the correlations between variable tokens independently. Each branch's backbone is the encoder of the vanilla Transformer. Subsequently, it merges the features from

the dual branches through a novel gated unit specifically crafted for TSF to make predictions. The overview of T2B-PE is shown in Figure 2. Next, we introduce the temporal token branch, variable token branch, and fusion module in turn.

Temporal token branch: This branch aims to handle the correlations between temporal tokens mentioned in Section IV-B. Specifically, we get H_l^{time} and $H_l^{en-time}$ through Equations 1 and 2. Then, we calculate the Q , K , and V of the attention mechanism. The computation of Q and K relies on H_l^{time} , while V is computed based on the $H_l^{en-time}$, expressed as:

$$\begin{aligned} Q^{time}, K^{time} &= \mathbf{FC}_{q/k}^{time}(H_l^{en-time}) \in \mathbb{R}^{T \times D}, \\ V^{time} &= \mathbf{FC}_v^{time}(H_l^{time}) \in \mathbb{R}^{T \times D}, \end{aligned} \quad (7)$$

where \mathbf{FC}_q^{time} , \mathbf{FC}_k^{time} and \mathbf{FC}_v^{time} are three fully connected layers. After obtaining Q , K , and V , the rest of the computation process remains consistent with the vanilla Transformer encoder. Firstly, these three embeddings are passed to an attention layer to produce the refined feature $\mathbf{A}(Q, K, V) = \text{softmax}(\frac{QK^T}{\sqrt{D}})V$, then the refined feature goes through a feedforward network (FFN) to obtain the output of the current layer, recorded as H_{l+1}^{time} which serves as the input embedding for the next layer. This process is repeated L times throughout the entire model. Finally, we obtain the output features of the temporal tokens branch, i.e., $H_{out}^{time} \in \mathbb{R}^{T \times D}$.

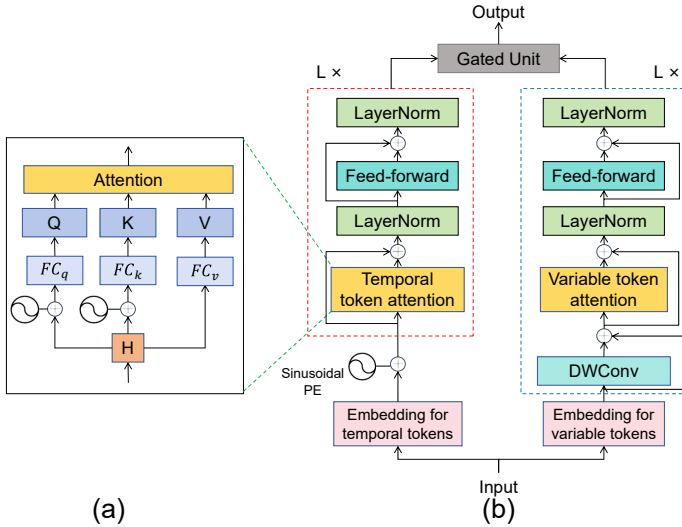


Fig. 2. Overview of T2B-PE. (a) details of temporal token attention. (b) structure of T2B-PE, the left branch is the temporal token branch, and the right branch is the variable token branch.

Variable token branch: This branch aims to handle the correlations between variable tokens mentioned in Section IV-C. Specifically, we first get H_l^{en-var} via Equation 5. Then, we calculate the Q , K , and V of this branch relying on H_l^{en-var} :

$$Q^{var}, K^{var}, V^{var} = \mathbf{FC}_{q/k/v}^{var}(H_l^{en-var}) \in \mathbb{R}^{N \times D}, \quad (8)$$

where \mathbf{FC}_q^{var} , \mathbf{FC}_k^{var} and \mathbf{FC}_v^{var} are three fully connected layers. The rest of the computation process is the same as the temporal token branch. Finally, we obtain the output features of the variable tokens branch, i.e., $H_{out}^{var} \in \mathbb{R}^{N \times D}$.

Fusion Module: In this module, we aim to merge the outputs

of the above two branches. Inspired by [39]–[41], we propose a novel gated unit specially designed for TSF to achieve this goal. The gated unit dynamically assesses the two branches' importance based on their outputs and performs weighted fusion. Specifically, we first use three fully connected layers to reshape the output features from both branches to the same shape:

$$\begin{aligned} F_{t_m} &= \mathbf{FC}_{t1}(H_{out}^{time}) \in \mathbb{R}^{T \times N}, \\ F_t &= \mathbf{FC}_{t2}(F_{t_m}^T) \in \mathbb{R}^{N \times S}, \\ F_v &= \mathbf{FC}_v(H_{out}^{var}) \in \mathbb{R}^{N \times S}, \end{aligned} \quad (9)$$

where $\mathbf{FC}_{t1} : \mathbb{R}^D \rightarrow \mathbb{R}^N$, $\mathbf{FC}_{t2} : \mathbb{R}^T \rightarrow \mathbb{R}^S$, $\mathbf{FC}_v : \mathbb{R}^D \rightarrow \mathbb{R}^S$ are three fully connected layers, F_{t_m} is the intermediate computation result, F_t represents the refined feature of the temporal token branch, F_v represents the refined features from the variable token branch. Subsequently, we employ the gated unit to fuse the output features from both branches:

$$\begin{aligned} G &= \sigma([F_t, F_v]W_f) \in \mathbb{R}^{N \times S}, \\ \hat{Y} &= G \odot F_v + (1 - G) \odot F_t, \end{aligned} \quad (10)$$

where $[\dots]$ denotes the operation of concatenation, $[F_t, F_v] \in \mathbb{R}^{N \times 2S}$, $W_f \in \mathbb{R}^{2S \times S}$, σ denotes a sigmoid operation, \odot denotes element-wise multiplication and $\hat{Y}^T \in \mathbb{R}^{S \times N}$ represents the final output. For simplicity, we let $\hat{Y} = \hat{Y}^T$.

To obtain accurate prediction results, we propose a new loss function to optimize the model, which introduces regularization terms mentioned in Equations 3 and 6 to the commonly-used MSE loss. This loss function is as follows:

$$\begin{aligned} \mathcal{L} &= \mathcal{L}_{MSE}(\hat{Y}, Y) + \alpha(\mathcal{L}_{sem}^{time} + \mathcal{L}_{sem}^{var}), \\ \text{s.t. } \mathcal{L}_{MSE}(\hat{Y}, Y) &= \frac{1}{N} \frac{1}{S} \sum_{i=1}^N \sum_{j=1}^S (\hat{Y}_{i,j} - Y_{i,j})^2, \end{aligned} \quad (11)$$

where Y represents the ground truth, \hat{Y} represents the predicted results, α is a hyperparameter and \mathcal{L}_{MSE} means the MSE loss. Through this equation, we can make the model better perceive the correlations of temporal tokens and variable tokens, thereby improving the performance. The pseudocode of our method is shown in Algorithm 1.

V. EXPERIMENTS

In this section, we first introduce the experimental settings. Next, we present the comparative experimental results on six benchmark datasets. Then, we conduct ablation studies to evaluate the effectiveness of each module in the proposed T2B-PE. Subsequently, we evaluate the hyperparameter sensitivity and the robustness of our method. Finally, we construct visualization experiments to evaluate our method.

A. Experimental settings

In this subsection, we introduce the datasets, the baselines, the implementation details, and the hyperparameter setting in turn.

Datasets: We utilize six real-world datasets, including ECL, ETTh2, Traffic, Weather in [15], Solar-Energy dataset in [42], and PEMS03 in [43]. For further details on datasets, refer to the Appendix.

TABLE II

FULL RESULTS FOR THE TSF TASK. THE INPUT SEQUENCE LENGTH FOR ALL BASELINE MODELS IS SET TO 96, AND THE PREDICTION LENGTHS INCLUDE EITHER {96, 192, 336, 720} OR {12, 24, 48, 96}. AMONG THE 10 BASELINE METHODS, EXCEPT FOR DSFORMER AND DBAFORMER, THE DATA ARE SOURCED FROM THE PAPER OF ITRANSFORMER. THE DATA FOR DSFORMER AND DBAFORMER ARE OBTAINED FROM THEIR RESPECTIVE PAPERS. THE “-” DENOTES THAT THE RESULT IS NOT REPORTED.

Models		Ours (Ours)	FEDformer (2022)	PatchTST (2023)	iTransformer (2023)	Crossformer (2023)	TimesNet (2023)	DLinear (2023)	DSformer (2023)	DBAFormer (2023)	SCINet (2022)	TIDE (2023)
Metric		MSE MAE	MSE MAE	MSE MAE	MSE MAE	MSE MAE	MSE MAE	MSE MAE	MSE MAE	MSE MAE	MSE MAE	MSE MAE
ETTh2	96	0.192 0.299	0.358 0.397	0.302 0.348	0.297 0.347	0.745 0.584	0.340 0.374	0.333 0.387	0.268 0.304	- -	0.707 0.621	0.400 0.440
	192	0.247 0.338	0.429 0.439	0.388 0.400	0.380 0.400	0.877 0.656	0.402 0.414	0.477 0.476	0.332 0.341	- -	0.860 0.689	0.528 0.509
	336	0.260 0.352	0.496 0.487	0.426 0.433	0.428 0.432	1.043 0.731	0.452 0.452	0.594 0.541	0.349 0.387	- -	1.000 0.744	0.643 0.571
	720	0.315 0.389	0.463 0.474	0.431 0.446	0.427 0.445	1.104 0.763	0.462 0.468	0.831 0.657	0.375 0.393	- -	1.249 0.838	0.874 0.679
	Avg	0.254 0.344	0.437 0.449	0.387 0.407	0.383 0.407	0.942 0.684	0.414 0.427	0.559 0.515	0.331 0.356	- -	0.954 0.723	0.611 0.550
ECL	96	0.136 0.233	0.193 0.308	0.195 0.285	0.148 0.240	0.219 0.314	0.168 0.272	0.197 0.282	0.163 0.264	0.176 0.280	0.247 0.345	0.237 0.329
	192	0.154 0.251	0.201 0.315	0.199 0.289	0.162 0.253	0.231 0.322	0.184 0.289	0.196 0.285	0.174 0.272	0.191 0.293	0.257 0.355	0.236 0.330
	336	0.168 0.266	0.214 0.329	0.215 0.305	0.178 0.269	0.246 0.337	0.198 0.300	0.209 0.301	0.187 0.287	0.194 0.297	0.269 0.369	0.249 0.344
	720	0.203 0.294	0.246 0.355	0.256 0.337	0.225 0.317	0.280 0.363	0.220 0.320	0.245 0.333	0.216 0.309	0.218 0.317	0.299 0.390	0.284 0.373
	Avg	0.165 0.261	0.214 0.327	0.216 0.304	0.178 0.270	0.244 0.334	0.192 0.295	0.212 0.300	0.185 0.283	0.195 0.297	0.268 0.365	0.251 0.344
Traffic	96	0.384 0.264	0.587 0.366	0.544 0.359	0.395 0.268	0.522 0.290	0.593 0.321	0.650 0.396	0.458 0.311	0.614 0.342	0.788 0.499	0.805 0.493
	192	0.399 0.275	0.604 0.373	0.540 0.354	0.417 0.276	0.530 0.293	0.617 0.336	0.598 0.370	0.467 0.323	0.630 0.340	0.789 0.505	0.756 0.474
	336	0.418 0.280	0.621 0.383	0.551 0.358	0.433 0.283	0.558 0.305	0.629 0.336	0.605 0.373	0.479 0.329	0.467 0.357	0.797 0.508	0.762 0.477
	720	0.456 0.299	0.629 0.382	0.586 0.375	0.467 0.302	0.589 0.328	0.640 0.350	0.645 0.394	0.512 0.342	0.658 0.352	0.841 0.523	0.719 0.449
	Avg	0.414 0.280	0.610 0.376	0.555 0.362	0.428 0.282	0.550 0.304	0.620 0.336	0.625 0.383	0.479 0.326	0.592 0.348	0.804 0.509	0.760 0.473
Weather	96	0.156 0.206	0.217 0.296	0.177 0.218	0.174 0.214	0.158 0.230	0.172 0.220	0.196 0.255	0.170 0.217	0.183 0.235	0.221 0.306	0.202 0.261
	192	0.206 0.251	0.276 0.336	0.225 0.259	0.221 0.254	0.206 0.277	0.219 0.261	0.237 0.296	0.215 0.257	0.252 0.292	0.261 0.340	0.242 0.298
	336	0.264 0.291	0.339 0.380	0.278 0.297	0.278 0.296	0.272 0.335	0.280 0.306	0.283 0.335	0.265 0.295	0.321 0.343	0.309 0.378	0.287 0.335
	720	0.318 0.336	0.403 0.428	0.354 0.348	0.358 0.349	0.398 0.418	0.365 0.359	0.345 0.381	0.322 0.342	0.337 0.371	0.377 0.427	0.351 0.386
	Avg	0.236 0.271	0.309 0.360	0.259 0.281	0.258 0.279	0.259 0.315	0.259 0.287	0.265 0.317	0.243 0.278	0.273 0.310	0.292 0.363	0.271 0.320
Solar-Energy	96	0.197 0.229	0.242 0.342	0.234 0.286	0.203 0.237	0.310 0.331	0.250 0.292	0.290 0.378	- -	- -	0.237 0.344	0.312 0.399
	192	0.232 0.256	0.285 0.380	0.267 0.310	0.233 0.261	0.734 0.725	0.296 0.318	0.320 0.398	- -	- -	0.280 0.380	0.339 0.416
	336	0.245 0.270	0.282 0.376	0.290 0.315	0.248 0.273	0.750 0.735	0.319 0.330	0.353 0.415	- -	- -	0.304 0.389	0.368 0.430
	720	0.246 0.272	0.357 0.427	0.289 0.317	0.249 0.275	0.769 0.765	0.338 0.337	0.356 0.413	- -	- -	0.308 0.388	0.370 0.425
	Avg	0.230 0.257	0.291 0.381	0.270 0.307	0.233 0.262	0.641 0.639	0.301 0.319	0.330 0.401	- -	- -	0.282 0.375	0.347 0.417
PEMS03	12	0.062 0.166	0.126 0.251	0.099 0.216	0.071 0.174	0.090 0.203	0.085 0.192	0.122 0.243	- -	- -	0.066 0.172	0.178 0.305
	24	0.083 0.190	0.149 0.275	0.142 0.259	0.093 0.201	0.121 0.240	0.118 0.223	0.201 0.317	- -	- -	0.085 0.198	0.257 0.371
	48	0.123 0.233	0.227 0.348	0.211 0.319	0.125 0.236	0.202 0.317	0.155 0.260	0.333 0.425	- -	- -	0.127 0.238	0.379 0.463
	96	0.156 0.266	0.348 0.434	0.269 0.370	0.160 0.270	0.262 0.367	0.228 0.317	0.457 0.515	- -	- -	0.178 0.287	0.490 0.539
	Avg	0.106 0.214	0.213 0.327	0.180 0.291	0.113 0.221	0.169 0.281	0.147 0.248	0.278 0.375	- -	- -	0.114 0.224	0.326 0.419

Baselines: We choose five popular Time Series Forecasting (TSF) methods for comparison, including (i) *FEDformer* [29], *PatchTST* [20] which are based on temporal tokens; (ii) *iTransformer* [15] which is based on variable tokens; and (iii) *Crossformer* [19] and *DSformer* [36] that are based on both temporal and variable tokens. Additionally, we introduce multiple recently proposed methods for comparison, including *TimesNet* [44], *DLinear* [45], *DBAFormer* [46], *SCINet* [43], and *TIDE* [47].

Implementation Details: We follow the standard setting as in [15]. The data undergo mean-std normalization before being input into the model and inverse mean-std normalization before output. All the experiments are implemented in PyTorch [48] and conducted on a single NVIDIA 4090 GPU. Mean Squared Error (MSE) and Mean Absolute Error (MAE) are used as evaluation metrics.

Hyperparameter Setting: In our experiments, we configure the number of attention layers, L , to 3 for the Weather dataset

and 4 for other datasets. The token dimension D is set to 512. The head number of multi-head attention is set to 8. The batch size is set to 16. Time series convolutional PE employs Depthwise Convolution (DWConv) [38] with a kernel size of 3, a stride of 1, and padding of 1. For all experiments, we utilize the Adam optimizer [49], with i) cosine learning rate decay following linear warm-up or ii) decay learning rate. The first strategy requires two hyperparameters: the warm-up length Len_w and the scaling factor f_s . When training reaches the m -th batch, the learning rate for this batch is:

$$lr = f_s * (D^{-0.5} * \min(m^{-0.5}, m * Len_w^{-1.5})). \quad (12)$$

The corresponding Len_w and f_s for each dataset are shown in Table III. Rows in Table III where Len_w and f_s are marked as ‘-’ indicate that this training strategy is not adopted for the dataset. Figure 3 shows the learning rate variation curve for this strategy, illustrating how the learning rate changes with the number of trained batches.

Algorithm 1 T2B-PE - Overall Architecture.**Require:** Input lookback time series $\mathbf{X} \in \mathbb{R}^{T \times N}$; input Length T ; predicted length S ; variates number N ; token dimension D ; the number of attention layers L .

- 1: $\mathbf{H}_1^{\text{time}} = \text{Embed}^t(\mathbf{X}) + PE_t$
- 2: $\mathbf{H}_1^{\text{var}} = \text{Embed}^v(\mathbf{X}^\top)$
- 3: \triangleright Temporal token branch.
- 4: **for** l **in** $\{1, \dots, L\}$:
 - 5: $\mathbf{H}_l^{\text{en-time}} = \mathbf{H}_l^{\text{time}} + PE_t$
 - 6: $\mathbf{Q}^{\text{time}}, \mathbf{K}^{\text{time}} = \text{FC}_{q/k}^{\text{time}}(\mathbf{H}_l^{\text{en-time}})$
 - 7: $\mathbf{V}^{\text{time}} = \text{FC}_v^{\text{time}}(\mathbf{H}_l^{\text{time}})$
 - 8: \triangleright Self-attention layer is applied on temporal tokens.
 - 9: \triangleright “LN” means “LayerNorm”, “SA” means “Self-Attn”, “FF” means “Feed-Forward”.
 - 10: $\mathbf{H}_l^{\text{time}} = \text{LN}(\mathbf{H}_l^{\text{time}} + \text{SA}(\mathbf{Q}^{\text{time}}, \mathbf{K}^{\text{time}}, \mathbf{V}^{\text{time}}))$
 - 11: $\mathbf{H}_{l+1}^{\text{time}} = \text{LN}(\mathbf{H}_l^{\text{time}} + \text{FF}(\mathbf{H}_l^{\text{time}}))$
 - 12: **End for**
 - 13: \triangleright Variable token branch.
 - 14: **for** l **in** $\{1, \dots, L\}$:
 - 15: $\mathbf{H}_l^{\text{en-var}} = \mathbf{H}_l^{\text{var}} + \text{DWConv}(\mathbf{H}_l^{\text{var}})$
 - 16: $\mathbf{Q}^{\text{var}}, \mathbf{K}^{\text{var}}, \mathbf{V}^{\text{var}} = \text{FC}_{q/k/v}^{\text{var}}(\mathbf{H}_l^{\text{en-var}})$
 - 17: \triangleright Self-attention layer is applied on variable tokens.
 - 18: $\mathbf{H}_l^{\text{var}} = \text{LN}(\mathbf{H}_l^{\text{en-var}} + \text{SA}(\mathbf{Q}^{\text{var}}, \mathbf{K}^{\text{var}}, \mathbf{V}^{\text{var}}))$
 - 19: $\mathbf{H}_{l+1}^{\text{var}} = \text{LN}(\mathbf{H}_l^{\text{var}} + \text{FF}(\mathbf{H}_l^{\text{var}}))$
 - 20: **End for**
 - 21: $\hat{\mathbf{Y}} = \text{Gated-Unit}(\mathbf{H}_{L+1}^{\text{time}}, \mathbf{H}_{L+1}^{\text{var}})$
 - 22: **Return** $\hat{\mathbf{Y}}$

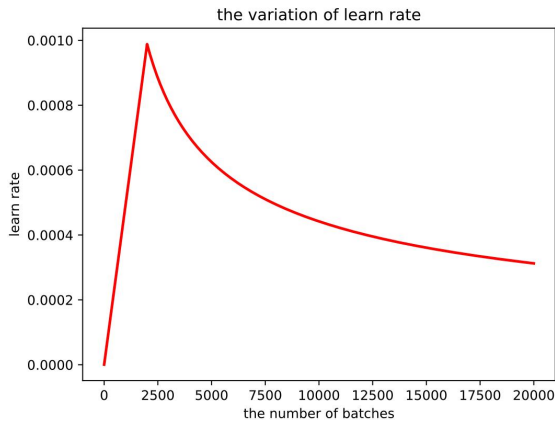


Fig. 3. The learning rate variation curve of the strategy of “cosine learning rate decay following linear warm-up” as the trained batch number varies.

TABLE III
HYPERPARAMETER SETTING FOR DIFFERENT DATASETS.

Dataset	Prediction Length	Len_{ws}	f_s	lr_{init}
ETTh2	96	2000	4.8e-4	-
	192	2000	6e-4	-
	336	2000	5.4e-4	-
	720	2000	9.3e-4	-
ECL	96	-	-	9.048e-4
	192	-	-	1.08e-3
	336	-	-	1.38e-3
	720	-	-	9.2e-4
Traffic	96	-	-	1.07e-3
	192	-	-	1.008e-3
	336	-	-	9.198e-4
	720	-	-	1.224e-3
Weather	96	2000	5.26e-4	-
	192	2000	5.52e-4	-
	336	2000	6e-4	-
	720	2000	5.95e-4	-
Solar -Energy	96	-	-	1.6e-4
	192	1100	5.371e-4	-
	336	1100	5.3e-4	-
	720	1100	5.664e-4	-
PEMS03	96	-	-	7.272e-4
	192	1100	6.292e-4	-
	336	1100	3.32e-4	-
	720	1100	4.224e-4	-

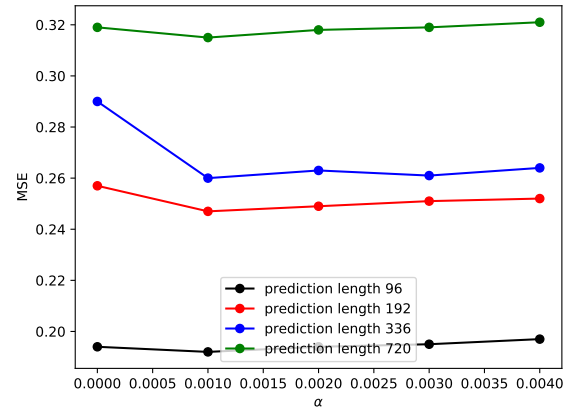


Fig. 4. The impact of α on ETTh2. The lookback length is 96 and the prediction lengths $\in \{96, 192, 336, 720\}$.

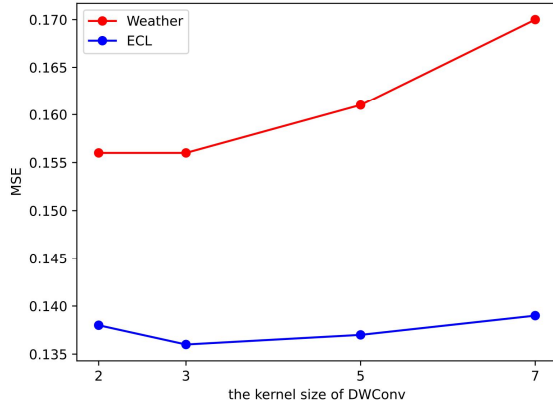


Fig. 5. The performance of time series convolutional PE with different kernel sizes. The results are recorded with the lookback length $T=96$ and the prediction length $S=96$.

TABLE IV
COMPARISON OF THE CHOICE OF THE DISTANCE ON WEATHER DATASET.
THE LOOKBACK LENGTH IS 96.

MSE/MAE	L1 Distance	L2 Distance
96	0.159/0.207	0.156/0.206
192	0.209/0.253	0.206/0.251
336	0.265/0.292	0.264/0.291
720	0.324/0.338	0.318/0.336
Avg	0.239/0.273	0.236/0.271

The second strategy requires one hyperparameter lr_{init} which is the initial learning rate for the training. When training reaches the k -th epoch, the learning rate for this batch is:

$$lr = lr_{init} * 0.5^k. \quad (13)$$

The corresponding lr_{init} for each dataset is shown in Table III. Rows in Table III where lr_{init} is marked as ‘-’ indicate that this training strategy is not adopted for the dataset. The total number of epochs is 40. The training process will stop early if the validation loss doesn’t decrease within three epochs.

B. Comparative Experimental Results

The comprehensive prediction results are presented in Table II, with the best outcomes highlighted in red and the second-best in blue. Lower MSE/MAE values indicate more accurate

TABLE V
THE PERFORMANCE OF OUR MODEL ON WEATHER DATASET WHEN Q , K , V OF THE TEMPORAL TOKEN BRANCH ARE COMPUTED BASED ON $H_l^{en-time}$. THE LOOKBACK LENGTH IS SET TO 96 AND THE PREDICTION LENGTHS $\in \{96, 192, 336, 720\}$.

MSE/MAE	our method	Q, K, V depend on $H_l^{en-time}$
96	0.156/0.206	0.167/0.209
192	0.206/0.251	0.220/0.273
336	0.264/0.291	0.282/0.312
720	0.318/0.336	0.340/0.357
Avg	0.236/0.271	0.252/0.288

predictions. Compared to other TSF models, our approach achieves state-of-the-art (SOTA) performance on all benchmark datasets. Meanwhile, the encoders of our model are the same as vanilla Transformers, where the only difference lies in the choice of PE. Experimental results show that SOTA performance can be achieved even with the simplest Transformer encoder structure, coupled with our PEs. The results demonstrate the superior performance of our proposed methods, where our PEs designed for temporal and variable tokens are effective.

C. Ablation Study

In this subsection, we analyze the effectiveness of each module proposed in this paper through ablation experiments.

The influence of α : Firstly, we explore the optimal value for α , a parameter used in Equation 11 to control the extent to which the model focuses on semantic PE. As shown in Figure 4, the optimal value for α is 0.001.

The kernel size of Time Series Convolutional PE: We test DWConv with kernel sizes of 2, 3, 5, and 7 to generate time series convolutional PE. The experimental results are shown in Figure 5. It can be seen from the figure that the kernel size of 3 is the optimal parameter setting.

The choice of the distance: In Equations 3 and 6, we need to measure the distance between the initial tokens’ similarity matrix and attention maps. The optional schemes include i) L1 distance, ii) L2 distance, iii) KL divergence [50], and iv) Wasserstein distance [51]. In our experiments, we find that KL divergence causes the training not to converge. As for the Wasserstein distance, since its computation requires the use of the GPU, we find that when the number of variables in the input data exceeds 200, the GPU memory becomes insufficient. Therefore, only L1 distance and L2 distance are suitable for experimentation. Specifically, we tested the two distances on the Weather dataset, and the specific results are shown in Table IV. The experimental results indicate that the L2 distance is more suitable for our method.

The calculation method of QKV in T-PE In Equation 7, the Q and K of the temporal token branch are calculated based on $H_l^{en-time}$, while V is calculated based on H_l^{time} . We briefly explain in Section IV-B why V cannot be calculated based on $H_l^{en-time}$. To verify the rationality of this concept, we conduct experiments to observe our method’s performance when V is also calculated based on $H_l^{en-time}$. From Table V, it can be seen that if Q , K , and V are all calculated based on $H_l^{en-time}$, it results in a significant decrease in our model’s performance. This demonstrates the reasonability of our design.

The choice of T-PE: We explore the PE design for T-PE. We experiment on Weather Dataset with the following T-PE designs: (i) No PE; (ii) Learnable PE [24]; (iii) Sinusoidal PE [25]; (iv) Enhanced learnable PE; (v) Enhanced sinusoidal PE; and (vi) Time series convolutional PE. Here, The enhanced PE refers to the strategy, that adds PE to the input embedding of each attention layer. We then apply the semantic PE to the six settings mentioned above. The experimental results are presented in Table VI. The experiment results show that T2B-PE with the enhanced sinusoidal PE and the semantic PE

TABLE VI

COMPARISON OF THE CHOICE OF T-PE ON ETTh2 DATASET. THE LOOKBACK LENGTH IS 96 AND THE PREDICTION LENGTHS $\in \{96, 192, 336, 720\}$.

MSE/MAE	No PE	Learnable PE	Sinusoidal PE	Enhanced learnable PE	Enhanced sinusoidal PE	Time series convolutional PE
w/o semantic PE						
96	0.309/0.377	0.216/0.337	0.214/0.330	0.197/0.305	0.194/0.303	0.208/0.333
192	0.348/0.392	0.270/0.373	0.273/0.374	0.259/0.348	0.257/0.346	0.267/0.371
336	0.400/0.420	0.305/0.395	0.301/0.387	0.294/0.382	0.290/0.373	0.294/0.393
720	0.432/0.454	0.336/0.420	0.327/0.414	0.326/0.408	0.319/0.400	0.327/0.418
Avg	0.372/0.411	0.282/0.381	0.279/0.376	0.269/0.361	0.265/0.356	0.274/0.379
with semantic PE						
96	0.303/0.375	0.202/0.331	0.203/0.325	0.194/0.304	0.192/0.299	0.201/0.321
192	0.344/0.388	0.262/0.369	0.260/0.367	0.249/0.347	0.247/0.338	0.260/0.363
336	0.398/0.415	0.299/0.386	0.292/0.380	0.270/0.357	0.260/0.352	0.292/0.381
720	0.429/0.452	0.329/0.415	0.320/0.408	0.317/0.393	0.315/0.389	0.324/0.404
Avg	0.369/0.408	0.273/0.375	0.269/0.370	0.258/0.350	0.254/0.344	0.269/0.367

TABLE VII

COMPARISON OF THE CHOICE OF V-PE ON ETTh2 DATASET. THE LOOKBACK LENGTH IS 96 AND THE PREDICTION LENGTHS $\in \{96, 192, 336, 720\}$.

MSE/MAE	No PE	Learnable PE	Sinusoidal PE	Enhanced learnable PE	Enhanced sinusoidal PE	Time series convolutional PE
w/o semantic PE						
96	0.313/0.370	0.205/0.320	0.199/0.308	0.203/0.311	0.201/0.312	0.194/0.303
192	0.357/0.377	0.269/0.368	0.269/0.364	0.268/0.359	0.262/0.357	0.257/0.346
336	0.412/0.415	0.299/0.383	0.295/0.382	0.296/0.381	0.298/0.385	0.290/0.373
720	0.439/0.441	0.328/0.406	0.325/0.414	0.329/0.416	0.323/0.413	0.319/0.400
Avg	0.380/0.401	0.275/0.369	0.272/0.367	0.274/0.367	0.271/0.367	0.265/0.356
with semantic PE						
96	0.305/0.359	0.201/0.306	0.199/0.306	0.200/0.308	0.196/0.307	0.192/0.299
192	0.360/0.371	0.265/0.358	0.264/0.358	0.260/0.350	0.261/0.356	0.247/0.338
336	0.403/0.407	0.290/0.381	0.290/0.380	0.291/0.380	0.288/0.377	0.260/0.352
720	0.433/0.430	0.318/0.397	0.313/0.394	0.317/0.395	0.315/0.396	0.315/0.389
Avg	0.375/0.392	0.269/0.361	0.267/0.360	0.267/0.358	0.265/0.359	0.254/0.344

has the best performance, validating the effectiveness of the designed T-PE.

The choice of V-PE: We explore the PE design for T-PE. The experimental settings are the same as T-PE. The results shown in Table VII indicate that T2B-PE with our time series convolutional PE and the semantic PE has the best performance, validating the designed V-PE's effectiveness.

The choice of fusion strategy: We explore the methods for fusing the outputs of the temporal token branch and the variable token branch. We choose the most commonly used FC fusion and our gating unit fusion for comparison. The FC fusion strategy directly uses one fully connected layer to fuse F_v and F_t in Equation 9. The results shown in Table VIII indicate that our gated unit fusion outperforms the FC fusion. This reflects the superiority of our gated unit.

Based on the results of the ablation experiments, we demonstrate the effectiveness of the designed framework.

D. Hyperparameter Sensitivity

We evaluate the hyperparameter sensitivity of our model concerning the following factors: the number of attention layers L of temporal token branch or variable token branch, and the hidden dimension D of temporal tokens or variable tokens. The results are shown in Figure 6. We find that the number of attention layers and the hidden dimension are not essentially favored to be as large as possible in our method.

E. Robustness of our method

We report the standard deviation of our method's performance under five runs with different random seeds in Table IX, which exhibits that the performance of our method is stable.

F. Visualization Analysis

In this subsection, we construct visualization experiments to evaluate our method.

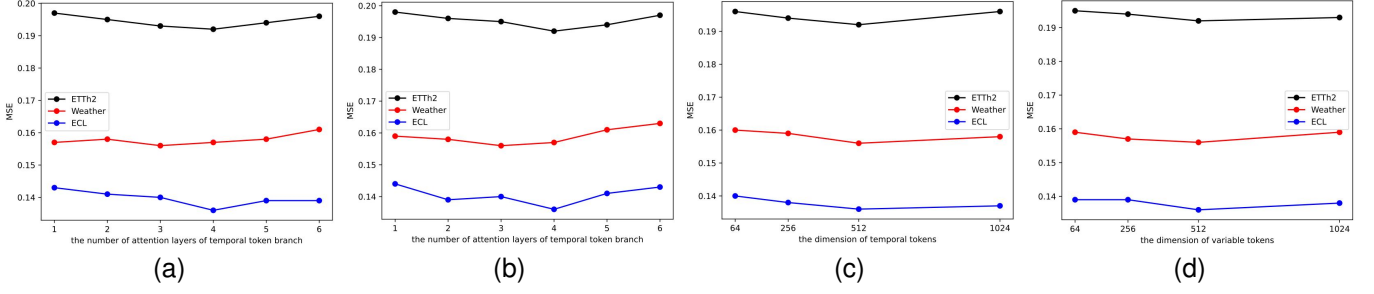


Fig. 6. The hyperparameter sensitivity of our model with respect to the number of attention layers L of temporal token branch or variable token branch, and the hidden dimension D of temporal tokens or variable tokens. The results are recorded with the lookback length $T=96$ and the prediction length $S=96$.

TABLE VIII
ABLATION STUDY OF THE FUSION STRATEGY ON ETTh2, WEATHER, AND ECL DATASET. THE LOOKBACK LENGTH IS 96 AND THE PREDICTION LENGTHS $\in \{96, 192, 336, 720\}$.

MSE/MAE	ETTh2	Weather	ECL
FC fusion			
96	0.195/0.302	0.162/0.212	0.144/0.241
192	0.253/0.348	0.215/0.252	0.160/0.257
336	0.267/0.359	0.271/0.292	0.173/0.271
720	0.319/0.393	0.330/0.344	0.212/0.303
Avg	0.259/0.351	0.251/0.276	0.172/0.268
Gated unit fusion			
96	0.192/0.299	0.156/0.206	0.136/0.233
192	0.247/0.338	0.206/0.251	0.154/0.251
336	0.260/0.352	0.264/0.291	0.168/0.266
720	0.315/0.389	0.318/0.336	0.203/0.294
Avg	0.254/0.344	0.236/0.271	0.165/0.261

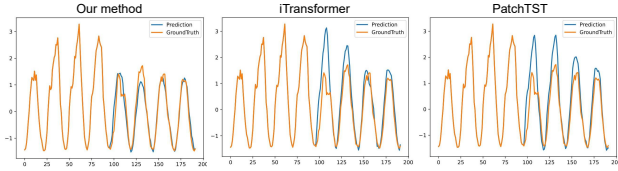


Fig. 7. Visualization of input-96-predict-96 results on the Traffic dataset.

Visualization of prediction results To provide a clear comparison among different models, we list the prediction showcases of three representative datasets in Figure 7, 8, 9, 10, 11 and 12, which are given by the following methods: Our method, iTransformer [15], PatchTST [20]. Among the various models, our method predicts the most precise future series

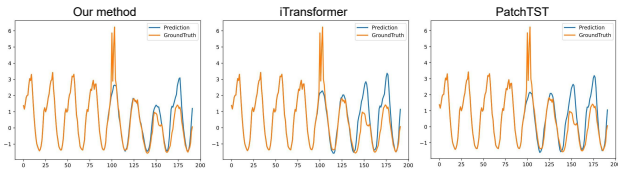


Fig. 8. Visualization of input-96-predict-96 results on the Traffic dataset.

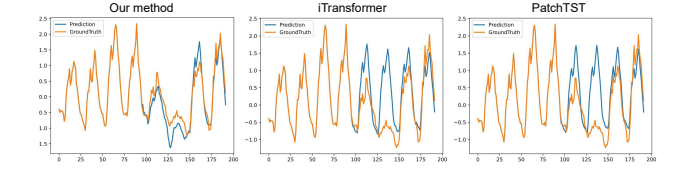


Fig. 9. Visualization of input-96-predict-96 results on the ECL dataset.

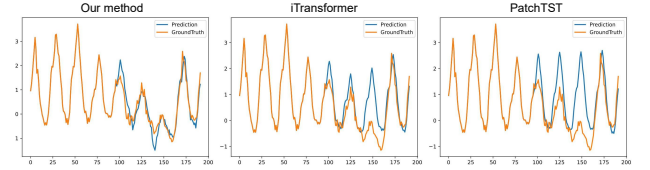


Fig. 10. Visualization of input-96-predict-96 results on the ECL dataset.

variations and exhibits superior performance.

The effectiveness of T-PE: We visualize the model performance and the importance of input temporal tokens after using different PEs, i.e., the sinusoidal PE, the learnable PE, and our T-PE. The importance of tokens has been widely applied in the field of computer vision [52], primarily used to measure the level of attention an algorithm gives to a specific token. We introduce this concept into the domain of TSF as a means to evaluate our algorithms. Ideally, the last few temporal tokens are more important, as they are closer to the prediction window [52]. The importance of most temporal tokens far from the

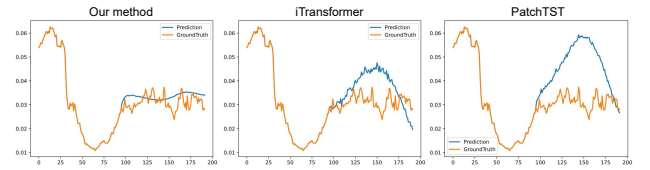


Fig. 11. Visualization of input-96-predict-96 results on the Weather dataset.

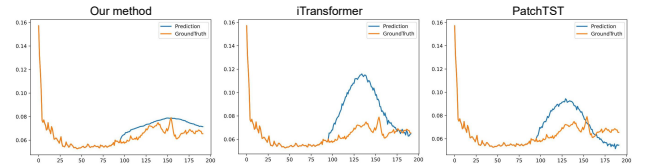


Fig. 12. Visualization of input-96-predict-96 results on the Weather dataset.

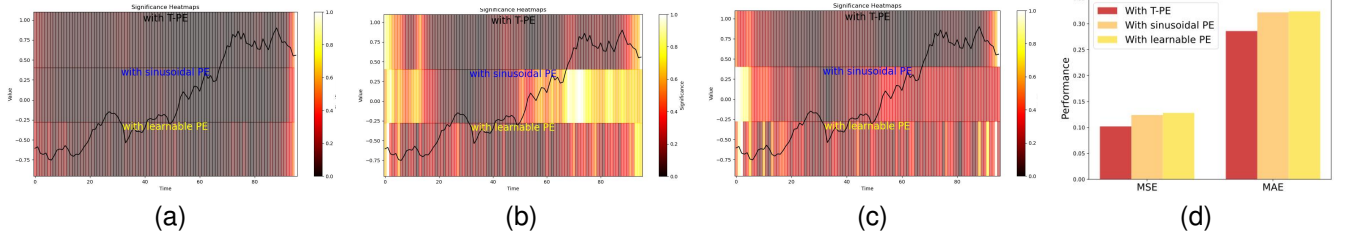


Fig. 13. Visualization of model performance and the importance of different input temporal tokens. The black line represents the input sequence, and the significance of tokens using T-PE, sinusoidal PE, or learnable PE is depicted in the background. The brighter areas indicate that the input tokens in those regions are more important. (a) First attention layer; (b) Second attention layer; (c) Third attention layer; (d) Prediction performance.

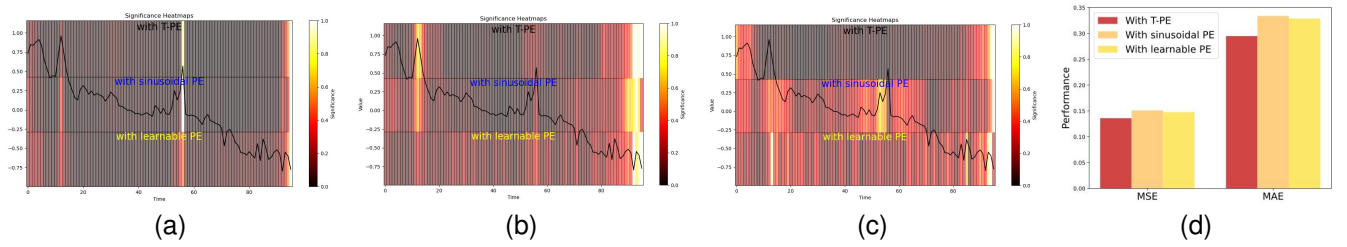


Fig. 14. Visualization of model performance and the importance of different input temporal tokens. The black line represents the input sequence, and the significance of tokens using T-PE, sinusoidal PE, or learnable PE is depicted in the background. The brighter areas indicate that the input tokens in those regions are more important. (a) First attention layer; (b) Second attention layer; (c) Third attention layer; (d) Prediction performance.

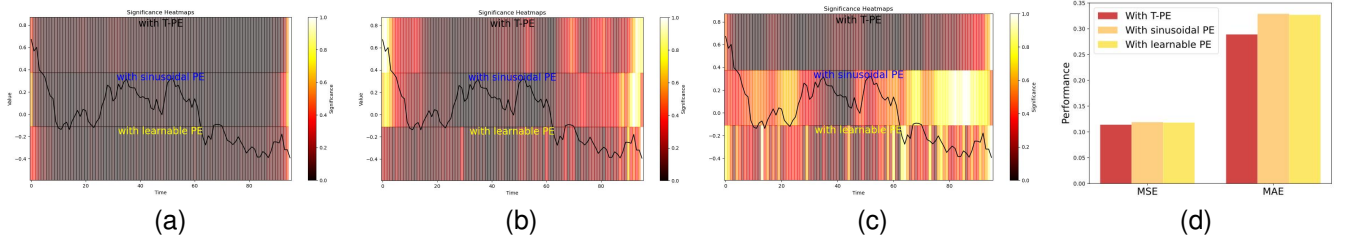


Fig. 15. Visualization of model performance and the importance of different input temporal tokens. The black line represents the input sequence, and the significance of tokens using T-PE, sinusoidal PE, or learnable PE is depicted in the background. The brighter areas indicate that the input tokens in those regions are more important. (a) First attention layer; (b) Second attention layer; (c) Third attention layer; (d) Prediction performance.

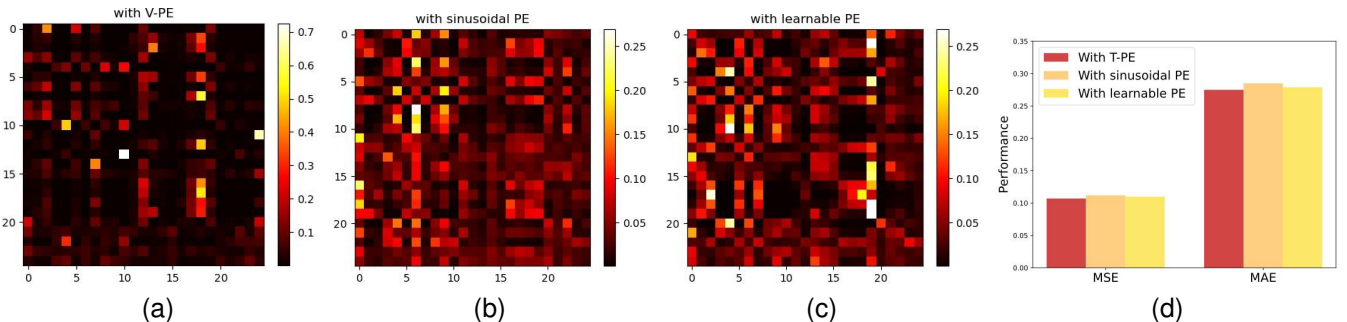


Fig. 16. Visualization of the model performance and the attention map. (a) The attention map of our model with V-PE; (b) The attention map of our model with sinusoidal PE. (c) The attention map of our model with learnable PE. (d) Prediction performance.

TABLE IX
ROBUSTNESS OF OUR METHOD'S PERFORMANCE. THE RESULTS ARE OBTAINED FROM FIVE RANDOM SEEDS. THE LOOKBACK LENGTH IS SET TO 96.

Dataset	ETTh2		Weather		ECL	
Prediction length	MSE	MAE	MSE	MAE	MSE	MAE
96	0.192±0.000	0.299±0.001	0.156±0.002	0.206±0.000	0.136±0.001	0.233±0.000
192	0.247±0.002	0.338±0.001	0.206±0.001	0.251±0.002	0.154±0.000	0.251±0.001
336	0.260±0.000	0.352±0.001	0.264±0.001	0.291±0.001	0.168±0.001	0.266±0.002
720	0.315±0.003	0.389±0.002	0.318±0.004	0.336±0.001	0.203±0.005	0.294±0.006

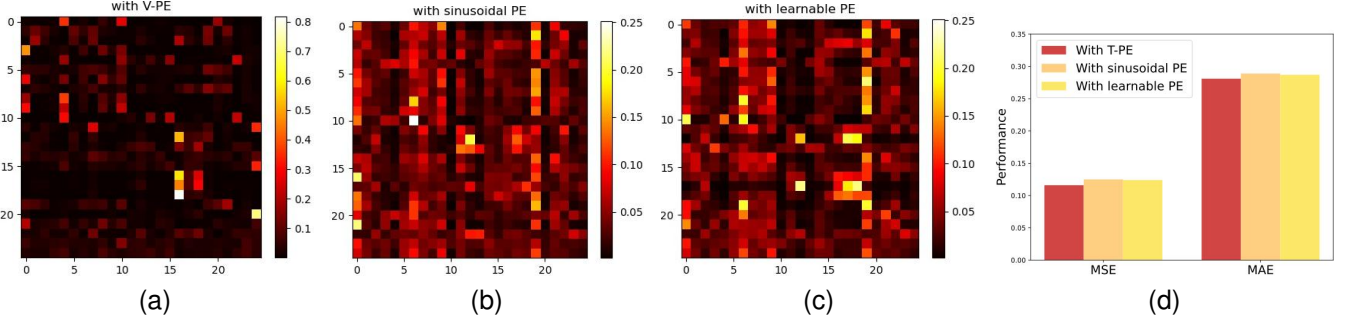


Fig. 17. Visualization of the model performance and the attention map. (a) The attention map of our model with V-PE; (b) The attention map of our model with sinusoidal PE. (c) The attention map of our model with learnable PE. (d) Prediction performance.

prediction window should be suppressed, especially when the overall trend of the input sequence is stable. The calculation of this importance is expressed as follows:

$$\text{Sign}(x_i) = \sum_{j=1}^T \text{Att}_{j,i}, \quad i = 1, 2, \dots, T, \quad (14)$$

where x_i is the i -th temporal token, T is the number of tokens, $\text{Att} \in \mathbb{R}^{T \times T}$ is the attention map, $\text{Sign}(x_i)$ is the sum of the elements in the i -th column of Att .

Figure 13, 14, 15 shows the visualization results. We can observe that (i) the token importance of the first attention layer using different PEs are almost the same; but (ii) in the second and third layers, the method using T-PE has higher token importance near the prediction window, lower token importance away from the prediction window, and lower MSE/MAE in predictions. This illustrates the effectiveness of our PEs.

The effectiveness of V-PE: To analyze the effectiveness of V-PE, we visualize the model performance and the attention map of the middle attention layer with three PEs, i.e., the sinusoidal PE, the learnable PE, and our T-PE. The results are shown in Figure 16, 17. From Figure 16, 17, we can observe that the model with V-PE focuses attention on fewer tokens, and has smaller MSE/MAE values. In contrast, the distribution of the attention map of the model with the sinusoidal PE or the learnable PE, is much more dispersed, resulting in larger MSE/MAE values. This indicates that V-PE encourages the model's attention maps to become more focused, improving the model's performance. In contrast, the sinusoidal PE and the learnable PE do not offer an advantage in this regard. The results demonstrate the advanced nature of V-PE.

VI. CONCLUSION

In this paper, we uncover intriguing properties of PE in TSF:

(i) The positional information injected by commonly used

PEs diminishes as the network depth increases; (ii) Enhancing positional information in deep networks is advantageous for improving the model's performance; (iii) PE based on the similarity between tokens can improve the model's performance. Motivated by these findings, we design better PEs for both temporal tokens and variable tokens, named T-PE and V-PE, respectively. Furthermore, we develop a Transformer-based dual-branch framework (T2B-PE), which first separately handles temporal tokens with T-PE and variable tokens with V-PE and then combines these two branches using the gating unit. Through extensive experiments, we validate the robustness and effectiveness of T2B-PE equipped with T-PE and V-PE.

REFERENCES

- [1] K. Abhishek, M. Singh, S. Ghosh, and A. Anand, "Weather forecasting model using artificial neural network," *Procedia Technology*, vol. 4, pp. 311–318, 2012.
- [2] Z. Karevan and J. A. Suykens, "Transductive lstm for time-series prediction: An application to weather forecasting," *Neural Networks*, vol. 125, pp. 1–9, 2020.
- [3] A. Agrawal, V. Kumar, A. Pandey, and I. Khan, "An application of time series analysis for weather forecasting," *International Journal of Engineering Research and Applications*, vol. 2, no. 2, pp. 974–980, 2012.
- [4] K. B. Debnath and M. Mourshed, "Forecasting methods in energy planning models," *Renewable and Sustainable Energy Reviews*, vol. 88, pp. 297–325, 2018.
- [5] O. Boussif, G. Boukachab, D. Assouline, S. Massaroli, T. Yuan, L. Benabbou, and Y. Bengio, "Improving* day-ahead* solar irradiance time series forecasting by leveraging spatio-temporal context," *Advances in Neural Information Processing Systems*, vol. 36, 2024.
- [6] R. Novo, P. Marocco, G. Giorgi, A. Lanzini, M. Santarelli, and G. Mattiazzo, "Planning the decarbonisation of energy systems: The importance of applying time series clustering to long-term models," *Energy Conversion and Management: X*, vol. 15, p. 100274, 2022.
- [7] H. Wang, T. Wang, S. Li, J. Zheng, W. Chen, and W. Chen, "Agree to disagree: Personalized temporal embedding and routing for stock forecast," *IEEE Transactions on Knowledge and Data Engineering*, 2024.
- [8] C.-H. L. Lee, A. Liu, and W.-S. Chen, "Pattern discovery of fuzzy time series for financial prediction," *IEEE Transactions on Knowledge and data Engineering*, vol. 18, no. 5, pp. 613–625, 2006.

- [9] H. Yan and H. Ouyang, "Financial time series prediction based on deep learning," *Wireless Personal Communications*, vol. 102, pp. 683–700, 2018.
- [10] Y. Fang, Y. Qin, H. Luo, F. Zhao, and K. Zheng, "Stwave+: A multi-scale efficient spectral graph attention network with long-term trends for disentangled traffic flow forecasting," *IEEE Transactions on Knowledge and Data Engineering*, 2023.
- [11] R. Li, F. Zhang, T. Li, N. Zhang, and T. Zhang, "Dmgan: Dynamic multi-hop graph attention network for traffic forecasting," *IEEE Transactions on Knowledge and Data Engineering*, 2022.
- [12] H. Wang, J. Chen, Z. Fan, Z. Zhang, Z. Cai, and X. Song, "St-expertnet: A deep expert framework for traffic prediction," *IEEE Transactions on Knowledge and Data Engineering*, 2022.
- [13] N. Wu, B. Green, X. Ben, and S. O'Banion, "Deep transformer models for time series forecasting: The influenza prevalence case," *arXiv preprint arXiv:2001.08317*, 2020.
- [14] B. Lim, S. Ö. Arik, N. Loeff, and T. Pfister, "Temporal fusion transformers for interpretable multi-horizon time series forecasting," *International Journal of Forecasting*, vol. 37, no. 4, pp. 1748–1764, 2021.
- [15] Y. Liu, T. Hu, H. Zhang, H. Wu, S. Wang, L. Ma, and M. Long, "itransformer: Inverted transformers are effective for time series forecasting," *arXiv preprint arXiv:2310.06625*, 2023.
- [16] J. Dong, H. Wu, H. Zhang, L. Zhang, J. Wang, and M. Long, "Simmtm: A simple pre-training framework for masked time-series modeling," *arXiv preprint arXiv:2302.00861*, 2023.
- [17] X. Chu, Z. Tian, B. Zhang, X. Wang, X. Wei, H. Xia, and C. Shen, "Conditional positional encodings for vision transformers," *arXiv preprint arXiv:2102.10882*, 2021.
- [18] P. Zeng, G. Hu, X. Zhou, S. Li, and P. Liu, "Seformer: a long sequence time-series forecasting model based on binary position encoding and information transfer regularization," *Applied Intelligence*, vol. 53, no. 12, pp. 15 747–15 771, 2023.
- [19] Y. Zhang and J. Yan, "Crossformer: Transformer utilizing cross-dimension dependency for multivariate time series forecasting," *ICLR*, 2023.
- [20] Y. Nie, N. H. Nguyen, P. Sinthong, and J. Kalagnanam, "A time series is worth 64 words: Long-term forecasting with transformers," *ICLR*, 2023.
- [21] J. Li, X. Hui, and W. Zhang, "Informer: Beyond efficient transformer for long sequence time-series forecasting," *arXiv: 2012.07436*, 2021.
- [22] Y. Lin, I. Koprinska, and M. Rana, "Springnet: Transformer and spring dtw for time series forecasting," in *Neural Information Processing: 27th International Conference, ICONIP 2020, Bangkok, Thailand, November 23–27, 2020, Proceedings, Part III* 27. Springer, 2020, pp. 616–628.
- [23] Y. Yang and J. Lu, "Foreformer: an enhanced transformer-based framework for multivariate time series forecasting," *Applied Intelligence*, vol. 53, no. 10, pp. 12 521–12 540, 2023.
- [24] A. Vaswani, N. Shazeer, N. Parmar, J. Uszkoreit, L. Jones, A. N. Gomez, L. Kaiser, and I. Polosukhin, "Attention is all you need," *NeurIPS*, 2017.
- [25] J. Devlin, M.-W. Chang, K. Lee, and K. Toutanova, "Bert: Pre-training of deep bidirectional transformers for language understanding," *arXiv preprint arXiv:1810.04805*, 2018.
- [26] T. M. Cover, *Elements of information theory*. John Wiley & Sons, 1999.
- [27] R. Steuer, J. Kurths, C. O. Daub, J. Weise, and J. Selbig, "The mutual information: detecting and evaluating dependencies between variables," *Bioinformatics*, vol. 18, no. suppl_2, pp. S231–S240, 2002.
- [28] H. Wu, J. Xu, J. Wang, and M. Long, "Autoformer: Decomposition transformers with Auto-Correlation for long-term series forecasting," *NeurIPS*, 2021.
- [29] T. Zhou, Z. Ma, Q. Wen, X. Wang, L. Sun, and R. Jin, "FEDformer: Frequency enhanced decomposed transformer for long-term series forecasting," *ICML*, 2022.
- [30] D. Liang, H. Zhang, D. Yuan, X. Ma, D. Li, and M. Zhang, "Does long-term series forecasting need complex attention and extra long inputs?" *arXiv preprint arXiv:2306.05035*, 2023.
- [31] Y. Zhao, Z. Ma, T. Zhou, M. Ye, L. Sun, and Y. Qian, "Gcformer: An efficient solution for accurate and scalable long-term multivariate time series forecasting," in *Proceedings of the 32nd ACM International Conference on Information and Knowledge Management*, 2023, pp. 3464–3473.
- [32] D. Du, B. Su, and Z. Wei, "Preformer: predictive transformer with multi-scale segment-wise correlations for long-term time series forecasting," in *ICASSP 2023-2023 IEEE International Conference on Acoustics, Speech and Signal Processing (ICASSP)*. IEEE, 2023, pp. 1–5.
- [33] S. Feng, C. Miao, K. Xu, J. Wu, P. Wu, Y. Zhang, and P. Zhao, "Multi-scale attention flow for probabilistic time series forecasting," *IEEE Transactions on Knowledge and Data Engineering*, 2023.
- [34] H. Xue and F. D. Salim, "Promptcast: A new prompt-based learning paradigm for time series forecasting," *IEEE Transactions on Knowledge and Data Engineering*, 2023.
- [35] P. Tang and X. Zhang, "Infomaxformer: Maximum entropy transformer for long time-series forecasting problem," *arXiv preprint arXiv:2301.01772*, 2023.
- [36] C. Yu, F. Wang, Z. Shao, T. Sun, L. Wu, and Y. Xu, "Dsformer: a double sampling transformer for multivariate time series long-term prediction," in *Proceedings of the 32nd ACM International Conference on Information and Knowledge Management*, 2023, pp. 3062–3072.
- [37] M. A. Islam, S. Jia, and N. D. Bruce, "How much position information do convolutional neural networks encode?" *arXiv preprint arXiv:2001.08248*, 2020.
- [38] F. Chollet, "Xception: Deep learning with depthwise separable convolutions," in *Proceedings of the IEEE conference on computer vision and pattern recognition*, 2017, pp. 1251–1258.
- [39] D. Yu, X. Li, C. Zhang, T. Liu, J. Han, J. Liu, and E. Ding, "Towards accurate scene text recognition with semantic reasoning networks," in *Proceedings of the IEEE/CVF conference on computer vision and pattern recognition*, 2020, pp. 12 113–12 122.
- [40] S. Fang, H. Xie, Y. Wang, Z. Mao, and Y. Zhang, "Read like humans: Autonomous, bidirectional and iterative language modeling for scene text recognition," in *Proceedings of the IEEE/CVF Conference on Computer Vision and Pattern Recognition*, 2021, pp. 7098–7107.
- [41] X. Yue, Z. Kuang, C. Lin, H. Sun, and W. Zhang, "Robustscanner: Dynamically enhancing positional clues for robust text recognition," in *European Conference on Computer Vision*. Springer, 2020, pp. 135–151.
- [42] G. Lai, W.-C. Chang, Y. Yang, and H. Liu, "Modeling long-and short-term temporal patterns with deep neural networks," *SIGIR*, 2018.
- [43] M. Liu, A. Zeng, M. Chen, Z. Xu, Q. Lai, L. Ma, and Q. Xu, "Scinet: time series modeling and forecasting with sample convolution and interaction," *NeurIPS*, 2022.
- [44] H. Wu, T. Hu, Y. Liu, H. Zhou, J. Wang, and M. Long, "Timesnet: Temporal 2d-variation modeling for general time series analysis," *ICLR*, 2023.
- [45] A. Zeng, M. Chen, L. Zhang, and Q. Xu, "Are transformers effective for time series forecasting?" *AAAI*, 2023.
- [46] J. Huang, M. Ma, Y. Dai, J. Hu, and S. Du, "Dbaformer: A double-branch attention transformer for long-term time series forecasting," *Human-Centric Intelligent Systems*, vol. 3, no. 3, pp. 263–274, 2023.
- [47] A. Das, W. Kong, A. Leach, R. Sen, and R. Yu, "Long-term forecasting with tide: Time-series dense encoder," *arXiv preprint arXiv:2304.08424*, 2023.
- [48] A. Paszke, S. Gross, F. Massa, A. Lerer, J. Bradbury, G. Chanan, T. Killeen, Z. Lin, N. Gimelshein, L. Antiga, A. Desmaison, A. Köpf, E. Yang, Z. DeVito, M. Raison, A. Tejani, S. Chilamkurthy, B. Steiner, L. Fang, J. Bai, and S. Chintala, "Pytorch: An imperative style, high-performance deep learning library," *NeurIPS*, 2019.
- [49] D. P. Kingma and J. Ba, "Adam: A method for stochastic optimization," *ICLR*, 2015.
- [50] Y. Bu, S. Zou, Y. Liang, and V. V. Veeravalli, "Estimation of kl divergence: Optimal minimax rate," *IEEE Transactions on Information Theory*, vol. 64, no. 4, pp. 2648–2674, 2018.
- [51] L. Rüschendorf, "The wasserstein distance and approximation theorems," *Probability Theory and Related Fields*, vol. 70, no. 1, pp. 117–129, 1985.
- [52] S. Ren, X. Yang, S. Liu, and X. Wang, "Sg-former: Self-guided transformer with evolving token reallocation," in *Proceedings of the IEEE/CVF International Conference on Computer Vision*, 2023, pp. 6003–6014.

VII. BIOGRAPHY SECTION



Jianqi Zhang received the M.S. degree in computer science and technology from Jilin University in 2019. He is currently a Ph.D. student at the University of Chinese Academy of Sciences. His research interests include time series forecasting and spatiotemporal predictive learning.



Fuchun Sun received the PhD degree in computer science and technology from Tsinghua University, Beijing, China, in 1997. He is currently a Professor with the Department of Computer Science and Technology and President of Academic Committee of the Department, Tsinghua University, deputy director of State Key Lab. of Intelligent Technology and Systems, Beijing, China. His research interests include intelligent control and robotics, information sensing and processing in artificial cognitive systems, and networked control systems. He was recognized as a Distinguished Young Scholar in 2006 by the Natural Science Foundation of China. He serves as Editor-in-Chief of International Journal on Cognitive Computation and Systems, and an Associate Editor for a series of international journals including the IEEE Transactions on Cognitive and Developmental Systems, the IEEE Transactions on Fuzzy Systems, and the IEEE Transactions on Systems, Man, and Cybernetic: Systems. He was elected an IEEE Fellow in 2019.



Jingyao Wang received the B.S. degree in Robotics Engineering from Beijing University of Technology, Beijing, China, in 2018. She is currently a postgraduate student at the University of Chinese Academy of Sciences. Her research interests include meta-learning, transfer learning and machine learning.



Hui Xiong is currently a Chair Professor at the Hong Kong University of Science and Technology (Guangzhou). Dr. Xiong's research interests include data mining, mobile computing, and their applications in business. Dr. Xiong received his PhD in Computer Science from University of Minnesota, USA. He has served regularly on the organization and program committees of numerous conferences, including as a Program Co-Chair of the Industrial and Government Track for the 18th ACM SIGKDD International Conference on Knowledge Discovery and Data Mining (KDD), a Program Co-Chair for the IEEE 2013 International Conference on Data Mining (ICDM), a General Co-Chair for the 2015 IEEE International Conference on Data Mining (ICDM), and a Program Co-Chair of the Research Track for the 2018 ACM SIGKDD International Conference on Knowledge Discovery and Data Mining. He received the 2021 AAAI Best Paper Award and the 2011 IEEE ICDM Best Research Paper award. For his outstanding contributions to data mining and mobile computing, he was elected an AAAS Fellow and an IEEE Fellow in 2020.



Wenwen Qiang received the M.S. degree in mathematics from China Agricultural University, Beijing, in 2018, and PhD degree in software engineering from the University of Chinese Academy of Sciences, Beijing, in 2022. Currently, he is an assistant professor with the Institute of Software Chinese Academy of Science. His research interests include transfer learning, self-supervised learning, and causal inference.



Fanjiang Xu is a Professor at the Institute of Software, Chinese Academy of Sciences. He received his B.Sc. and M.Sc. degrees in computer science both from National University of Defense Technology and his Ph.D. degree in computer science from Huazhong University of Science and Technology. His research interests include intelligent information processing and integration.



Changwen Zheng received the B.S. degree in mathematics from Huazhong Normal University in 1992 and the Ph.D. degree in computer science and technology from Huazhong University of Science and Technology in 2003, respectively. He is currently a Professor with the Institute of Software Chinese Academy of Sciences. His current research interests include route planning, evolutionary computation, and neural networks.

Intriguing Properties of Positional Encoding in Time Series Forecasting-Appendix

Jianqi Zhang, Jingyao Wang, Wenwen Qiang, Fanjiang Xu, Changwen Zheng, Fuchun Sun, *Fellow, IEEE*, and Hui Xiong, *Fellow, IEEE*

The appendix provides supplemental information and additional details to support the main findings and the method presented in this paper. It is divided into three sections: Appendix A lists all datasets mentioned in the paper; Appendix B describes more implementation details; Appendix C further presents the detailed content of motivation experiments; and Appendix D demonstrates the enhancements to other algorithms achieved by applying the proposed T-PE or V-PE.

APPENDIX A DATASET DESCRIPTIONS

In this paper, we performed tests using six real-world datasets. These include: (1) ETTh2 [1], which encompasses seven variables related to electricity transformers, gathered hourly from July 2016 to July 2018. (2) Weather [2], covering 21 meteorological variables, was recorded at 10-minute intervals in 2020 by the Max Planck Institute for Biogeochemistry's Weather Station. (3) ECL [2], detailing the hourly electrical usage of 321 customers. (4) Traffic [2], which compiles data on the hourly occupancy rates of roads, monitored by 862 sensors in the San Francisco Bay area's freeways, spanning from January 2015 to December 2016. (5) Solar-Energy [3], documenting the solar energy output from 137 photovoltaic (PV) plants in 2006, with data points every 10 minutes. (6) PEMS03 [4], which includes data on California's public traffic network, collected in 5-minute intervals.

We follow the same data processing and train-validation-test set split protocol used in iTransformer [5], where the train, validation, and test datasets are strictly divided according to chronological order to make sure there are no data leakage issues. As for the forecasting settings, the lookback length for datasets ETTh2, Weather, ECL, Solar-Energy, and Traffic is set to 96, while their prediction length varies in {96, 192, 336, 720}. For PEMS03, the lookback length is set to 96, and their prediction length varies in {12, 24, 36, 48} which is the same as SCINet [4]. The details of the datasets are provided in Table I.

APPENDIX B MORE IMPLEMENTATION DETAILS

In this section, we provide more details about our method. Specifically, we first illustrate the process of obtaining time tokens and variable tokens. Then, we introduce how to calculate the Mutual Information (MI) between two variables.

This paper was produced by the IEEE Publication Technology Group. They are in Piscataway, NJ.

Manuscript received April 19, 2021; revised August 16, 2021.

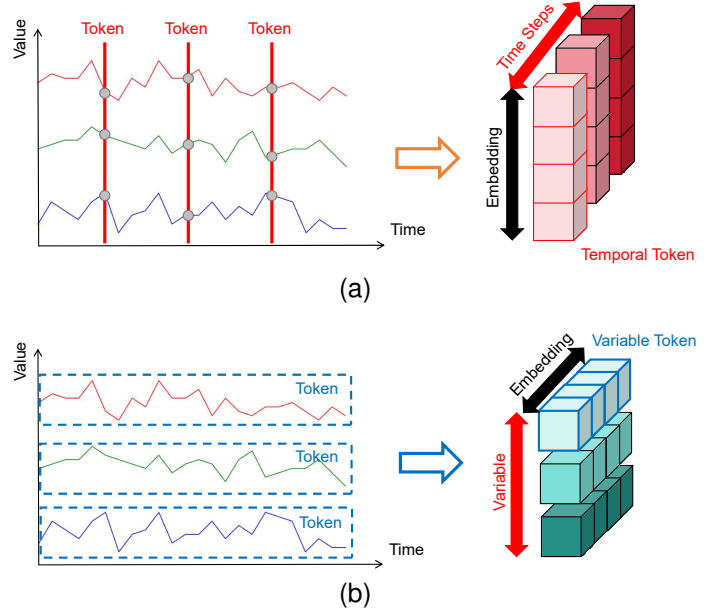


Fig. 1. Visualization of the generation of temporal tokens and variable tokens.

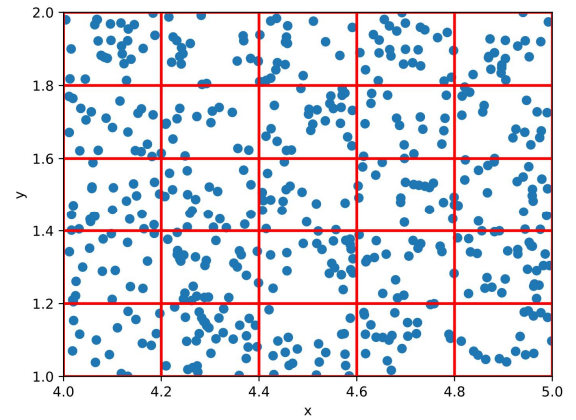


Fig. 2. An example illustration of variable xy being uniformly divided into an $M \times M$ grid of regions.

A. Visualize the acquisition of different tokens

Our method deals with two types of tokens: (i) temporal tokens, which contain all variables of the same timestamp; and (ii) variable tokens, which contain all input time points for a specific variable. We have visualized the generation of these two types of tokens in Figure 1 to aid readers' understanding.

TABLE I

DETAILED DATASET DESCRIPTIONS. DIM DENOTES THE VARIATE NUMBER OF EACH DATASET. DATASET SIZE DENOTES THE TOTAL NUMBER OF TIME POINTS IN (TRAIN, VALIDATION, TEST) SPLIT RESPECTIVELY. PREDICTION LENGTH DENOTES THE FUTURE TIME POINTS TO BE PREDICTED AND FOUR PREDICTION SETTINGS ARE INCLUDED IN EACH DATASET. FREQUENCY DENOTES THE SAMPLING INTERVAL OF TIME POINTS.

Dataset	Dim	Prediction Length	Dataset Size	Frequency	Information
ETTh2	7	{96, 192, 336, 720}	(8545, 2881, 2881)	Hourly	Electricity
Weather	21	{96, 192, 336, 720}	(36792, 5271, 10540)	10min	Weather
ECL	321	{96, 192, 336, 720}	(18317, 2633, 5261)	Hourly	Electricity
Traffic	862	{96, 192, 336, 720}	(12185, 1757, 3509)	Hourly	Transportation
Solar-Energy	137	{96, 192, 336, 720}	(36601, 5161, 10417)	10min	Energy
PEMS03	358	{12, 24, 48, 96}	(15617, 5135, 5135)	5min	Transportation

B. Calculation of the Mutual Information Between Two Variables

Considering two variables, x and y , the calculation method for the Mutual Information between them is:

$$I(x, y) = \sum p(x, y) \log \frac{p(x, y)}{p(x)p(y)} \quad (1)$$

However, since x and y are continuous variables, their probabilities cannot be directly estimated. To calculate MI between continuous variables, the academic community often uses the histogram-based method to estimate their probabilities [6]. Next, we provide a detailed introduction to this method.

Firstly, we flatten x and y into two one-dimensional vectors:

$$\begin{aligned} x &= \{x_i\} \quad i = 1, 2, \dots, P, \\ y &= \{y_i\} \quad i = 1, 2, \dots, P. \end{aligned} \quad (2)$$

Given an origin o and a width h , the bins of the histogram for the variable x are defined through the intervals $[o + mh, o + (m + 1)h]$ with $m = 0, \dots, M - 1$. The data in x are thus partitioned into M discrete bins a_i and k_i denotes the number of measurements that lie within the bin a_i . The probabilities $p(x)$ are then approximated by the corresponding relative frequencies of occurrence:

$$p(x) = p(a_i) = \frac{k_i}{P}. \quad (3)$$

Similarly, y is also divided into M discrete bins b_j . The probabilities $p(y)$ is calculated by:

$$p(y) = p(b_j) = \frac{k_j}{P}. \quad (4)$$

By concatenating x and y , we can obtain the joint variable xy :

$$xy = \{x_i, y_i\} \quad i = 1, 2, \dots, P. \quad (5)$$

Similarly, xy is also divided into $M \times M$ discrete bins (See Figure 2). By counting the number of points in each bin region, we can obtain the joint probability distribution of x and y :

$$p(x, y) = p(a_i, b_j) = \frac{k_{ij}}{P}, \quad (6)$$

where k_{ij} denotes the number of points where x lines in a_i and y in b_j . By substituting Equations 3, 4 and 6 into 1, we can obtain the formula for calculating the MI between the discrete

$$I(x, y) = \sum \frac{k_{ij}}{P} \log \frac{k_{ij} * P}{k_i * k_j} \quad (7)$$

APPENDIX C

MORE DETAILS ON THE MOTIVATION EXPERIMENT

In this section, we present the complete results of the second and third experiments in the motivation section of the main text (Table II). The specific experimental settings can be referred to in Section 3 of the main text. The experiment results show that both enhanced PE and semantic PE can improve the performance of current models of time series forecasting (TSF).

APPENDIX D

PERFORMANCE ENHANCEMENT AFTER USING T-PE OR V-PE

In this section, we apply the proposed T-PE or V-PE to three algorithms: vanilla Transformer [7], iTransformer [5], and PatchTST [8]. We evaluate these three algorithms on the Weather dataset and the ECL dataset to observe the performance improvement after incorporating the proposed PEs. Vanilla Transformer and PatchTST deal with temporal tokens, so only T-PE can be used. iTransformer deals with variable tokens, so only V-PE can be used. The experimental results are shown in Table III.

TABLE II
EXPERIMENTAL RESULTS ON WEATHER DATASET WITH DIFFERENT POSITIONAL ENCODINGS (PEs). THE LOOKBACK LENGTH FOR ALL MODELS IS SET TO 96, AND THE PREDICTION LENGTHS $\in \{96, 192, 336, 720\}$.

MSE/MAE	Dataset	Prediction length	Original	+enhanced PE	+semantic PE
Transformer +sinusoidal PE	Weather	96	0.224/0.317	0.194/0.286	0.200/0.289
		192	0.312/0.397	0.282/0.351	0.293/0.372
		336	0.383/0.434	0.382/0.416	0.372/0.406
		720	0.596/0.579	0.496/0.518	0.523/0.534
		Avg	0.379/0.432	0.339/0.393	0.347/0.400
	ECL	96	0.322/0.405	0.276/0.368	0.301/0.382
		192	0.332/0.413	0.288/0.379	0.308/0.387
		336	0.336/0.417	0.294/0.384	0.316/0.394
		720	0.340/0.421	0.299/0.392	0.326/0.401
		Avg	0.333/0.414	0.289/0.381	0.313/0.391
PatchTST +learnable PE	Weather	96	0.177/0.218	0.172/0.208	0.175/0.207
		192	0.225/0.259	0.211/0.251	0.220/0.254
		336	0.278/0.297	0.273/0.293	0.276/0.297
		720	0.354/0.348	0.344/0.345	0.347/0.345
		Avg	0.259/0.281	0.250/0.274	0.255/0.276
	ECL	96	0.195/0.285	0.191/0.283	0.193/0.283
		192	0.199/0.289	0.195/0.285	0.196/0.285
		336	0.215/0.305	0.209/0.299	0.211/0.302
		720	0.256/0.337	0.249/0.325	0.252/0.329
		Avg	0.216/0.304	0.211/0.298	0.213/0.300
iTransformer +sinusoidal PE	Weather	96	0.171/0.211	0.166/0.210	0.161/0.209
		192	0.214/0.252	0.210/0.252	0.211/0.252
		336	0.277/0.295	0.280/0.293	0.269/0.293
		720	0.359/0.353	0.358/0.351	0.352/0.348
		Avg	0.255/0.278	0.254/0.277	0.248/0.276
	ECL	96	0.146/0.240	0.143/0.239	0.139/0.236
		192	0.160/0.252	0.156/0.252	0.155/0.251
		336	0.176/0.268	0.173/0.267	0.171/0.266
		720	0.214/0.307	0.210/0.305	0.207/0.300
		Avg	0.174/0.267	0.171/0.266	0.168/0.263
iTransformer +learnable PE	Weather	96	0.163/0.207	0.158/0.208	0.157/0.205
		192	0.211/0.251	0.210/0.252	0.208/0.249
		336	0.273/0.294	0.270/0.291	0.269/0.295
		720	0.358/0.353	0.356/0.351	0.346/0.346
		Avg	0.251/0.276	0.249/0.276	0.245/0.274
	ECL	96	0.146/0.238	0.144/0.238	0.142/0.236
		192	0.161/0.253	0.158/0.253	0.156/0.252
		336	0.177/0.268	0.174/0.267	0.172/0.266
		720	0.220/0.312	0.215/0.309	0.210/0.306
		Avg	0.176/0.268	0.173/0.267	0.170/0.265

TABLE III

THE PERFORMANCE OF APPLYING T-PE OR V-PE TO DIFFERENT MODELS ON THE WEATHER DATASET AND THE ECL DATASET. THE LOOKBACK LENGTH FOR ALL MODELS IS SET TO 96, AND THE PREDICTION LENGTHS $\in \{96, 192, 336, 720\}$.

MSE/MAE	Dataset	Prediction length	Original	+T-PE or V-PE
Transformer	Weather	96	0.224/0.317	0.184/0.275
		192	0.312/0.397	0.255/0.311
		336	0.383/0.434	0.344/0.372
		720	0.596/0.579	0.480/0.498
		Avg	0.379/0.432	0.316/0.364
	ECL	96	0.322/0.405	0.270/0.362
		192	0.332/0.413	0.282/0.374
		336	0.336/0.417	0.288/0.382
		720	0.340/0.421	0.291/0.387
		Avg	0.333/0.414	0.283/0.376
PatchTST	Weather	96	0.177/0.218	0.171/0.208
		192	0.225/0.259	0.209/0.255
		336	0.278/0.297	0.273/0.294
		720	0.354/0.348	0.342/0.340
		Avg	0.259/0.281	0.249/0.274
	ECL	96	0.195/0.285	0.186/0.281
		192	0.199/0.289	0.192/0.283
		336	0.215/0.305	0.203/0.291
		720	0.256/0.337	0.245/0.318
		Avg	0.216/0.304	0.207/0.293
iTransformer	Weather	96	0.174/0.214	0.159/0.208
		192	0.221/0.254	0.210/0.252
		336	0.278/0.296	0.266/0.293
		720	0.358/0.349	0.350/0.345
		Avg	0.258/0.279	0.246/0.275
	ECL	96	0.148/0.240	0.141/0.235
		192	0.162/0.253	0.156/0.252
		336	0.178/0.269	0.169/0.264
		720	0.225/0.317	0.209/0.305
		Avg	0.178/0.270	0.169/0.264

REFERENCES

- [1] J. Li, X. Hui, and W. Zhang, “Informer: Beyond efficient transformer for long sequence time-series forecasting,” *arXiv: 2012.07436*, 2021.
- [2] H. Wu, J. Xu, J. Wang, and M. Long, “Autoformer: Decomposition transformers with Auto-Correlation for long-term series forecasting,” *NeurIPS*, 2021.
- [3] G. Lai, W.-C. Chang, Y. Yang, and H. Liu, “Modeling long-and short-term temporal patterns with deep neural networks,” *SIGIR*, 2018.
- [4] M. Liu, A. Zeng, M. Chen, Z. Xu, Q. Lai, L. Ma, and Q. Xu, “Scinet: time series modeling and forecasting with sample convolution and interaction,” *NeurIPS*, 2022.
- [5] Y. Liu, T. Hu, H. Zhang, H. Wu, S. Wang, L. Ma, and M. Long, “itransformer: Inverted transformers are effective for time series forecasting,” *arXiv preprint arXiv:2310.06625*, 2023.
- [6] A. J. Butte and I. S. Kohane, “Mutual information relevance networks: functional genomic clustering using pairwise entropy measurements,” in *Biocomputing 2000*. World Scientific, 1999, pp. 418–429.
- [7] A. Vaswani, N. Shazeer, N. Parmar, J. Uszkoreit, L. Jones, A. N. Gomez, L. Kaiser, and I. Polosukhin, “Attention is all you need,” *NeurIPS*, 2017.
- [8] Y. Nie, N. H. Nguyen, P. Sinthong, and J. Kalagnanam, “A time series is worth 64 words: Long-term forecasting with transformers,” *ICLR*, 2023.